Lubrication in polymer-brush bilayers in the weak interpenetration regime: Molecular dynamics simulations and scaling theories

Parth Rakesh Desai and Siddhartha Das*
Department of Mechanical Engineering, University of Maryland, College Park, Maryland 20742, USA

(Received 25 May 2018; published 28 August 2018)

We conduct molecular dynamics (MD) simulations and develop scaling laws to quantify the lubrication behavior of weakly interpenetrated polymer brush bilayers in the presence of an external shear force. The weakly interpenetrated regime is characterized by $1 < d_g/d_0 < 2$, where d_g is the gap between the opposing surfaces (where the brushes are grafted) and d_0 is the unperturbed brush height. MD simulations predict that in the shear thinning regime, characterized by a larger shear force or a large Weissenberg number (W), $R_g^2 \sim W^{0.19}$ and $\eta \sim W^{-0.38}$, where R_g is the chain extension in the direction of the shear and η is the viscosity. These scaling behaviors, which are distinctly different from that witnessed in strongly compressed regime (for such a regime, characterized by $d_g/d_0 < 1$, $R_g^2 \sim W^{0.53}$, and $\eta \sim W^{-0.46}$), match excellently with those predicted by our scaling theory.

DOI: 10.1103/PhysRevE.98.022503

I. INTRODUCTION

Functionalizing surfaces by grafting them with polymer molecules in "brush"-like configurations [1–6] have been employed in a large number of applications such as drug delivery [7,8], oil recovery [9], emulsion stabilization [10], wettability modulation of coatings [11], developing anti-biofouling crystals [12], sensing of ions and biomolecules [13–17], current rectification [18], fabrication of nanofluidic diodes [19,20], and many more. In "brush" configuration the polymer molecules stretch away from the grafted surface, and several of these applications harness this stretching behavior in response to environmental cues (e.g., salt concentration, solvent quality, *p*H, etc.). An extremely important variant of the problem is the case of interpenetrating polymer brushes, where the polymer brushes grafted at two opposing walls interact [21]. In other words the distance of separation between the opposing grafting surface (d_g) is less than $2d_0$ (where d_0 is the height of the unperturbed brushes). Such interpenetrated polymer and polyelectrolyte (PE) brush systems have been extensively explored, often with the intention to better understand the large lubricity that characterizes this regime and makes such interpenetrated polymer brush systems employable in applications such as friction reduction [22–30] and fabrication of lubricated coatings [31] and artificial hip and knee joints [32,33].

The majority of the studies on interpenetrated polymer and PE brushes have focused on strongly compressed brush bilayers (BBLs) characterized by $d_g < d_0$ (i.e., there is an actual physical compression) [26–30,34–60]. This has stemmed from the fact that such highly compressed brushes being the best representation of the conditions in the human hip and knee joints are ideal to probe for facilitating the fabrication of the artificial joints. Kreer in his recent review has nicely summarized several key findings of these papers [21]. Very recently we extended these calculations for a different compression regime [61,62]: we considered a weakly interpenetrated regime characterized by $1 < d_g/d_0 < 2$. We conducted molecular dynamics (MD) simulations and scaling analyses to establish a completely different scaling behavior of the equilibrium configuration of the polymer and PE brushes in comparison to those witnessed for highly compressed regimes.

In this paper, we carry out MD simulations and scaling analysis to study the lubrication behavior of the weakly interpenetrated polymer BBLs in the presence of an applied shear. We establish through MD simulations that in the shear thinning regime, characterized by the application of a large shear stress or $W \gg 1$ (where W is the Weissenberg number, which represents the dimensionless shear rate and can be expressed as $W = \dot{\gamma}\tau$ with $\dot{\gamma}$ being the shear rate and τ being the polymer relaxation time), $\eta \sim W^{-0.38}$ and $R_g^2 \sim W^{0.19}$ (where η is the viscosity and R_g is the chain extension in the direction of the applied shear). These scaling conditions are distinctly deviated for the brushes in the highly compressed regime, where one witnesses $\eta \sim W^{-0.46}$ and $R_g^2 \sim W^{0.53}$ [21,34,35]. We also carry out an extensive theoretical analysis and obtain excellent match with our MD predictions. We discuss that such a match for the variation of the viscosity occurs only when, motivated by the findings of the MD simulations, we consider that even at very small shear rate ($\dot{\gamma}$) the shear stress (f_s) varies nonlinearly with the shear rate, i.e., $f_s \sim \dot{\gamma}^{0.81}$. On the other hand, the match for the variation of the extension is ensured by accounting for the contribution of both the interpenetrated and the noninterpenetrated (brushlike) segments of the polymer brushes.

II. MOLECULAR DYNAMICS SIMULATIONS: METHODOLOGY

We perform MD simulations using the LAMMPS software package [63]. We consider a system of two opposing plates,

*sidd@umd.edu

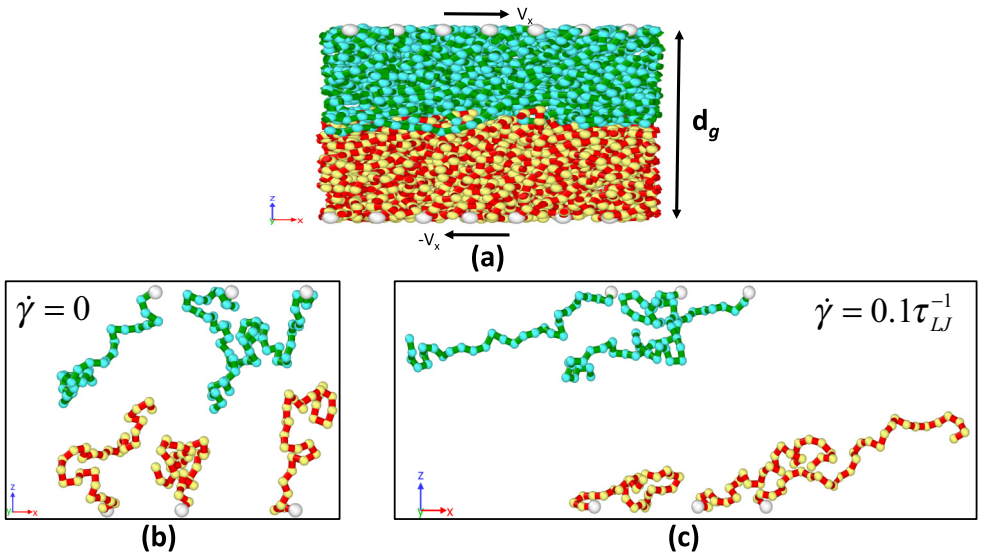

FIG. 1. (a) Snapshots showing the polymer BBLs in presence of a large shear ($\dot{\gamma} = 0.1\tau_{LJ}^{-1}$). (b) The polymer BBL in absence of the shear. (c) The polymer BBL in presence of the large shear ($\dot{\gamma} = 0.1\tau_{LJ}^{-1}$). In (b) and (c) we intentionally select only three polymer brush molecules from the top and the bottom plate of the configuration shown in (a) in order to clearly visualize the massive deformation of the brushes in presence of the shear. In panels (a)–(c) we consider $d_g/d_0 = 1.2$.

with $M = 49$ polymer chains grafted on each plate. Each polymer chain consists of $N = 30$ monomers. The polymers are grafted in a uniform square lattice with a grafting density $\rho_g = 0.1460\,\sigma_{LJ}^{-2} = 5\rho_g{}^*$, where σ_{LJ} is the Lennard-Jones length unit and $\rho_g{}^*$ is the critical grafting density at which the polymer crosses over from the mushroom to the brush regime.

We use the Kremer-Grest (KG) bead spring model to simulate the polymer chains [64–66]. In the KG model the monomers of a polymer chain are connected by a FENE bond and the nonbonded monomers interact via the shifted and truncated Lennard-Jones potential (LJ) potential. The detailed equations for these potentials are provided in our previous paper [61] and are not repeated here for the sake of brevity. The brushes are grafted at $z = 0$ and $z = d_g$ (see Fig. 1). Additionally, to prevent the monomers from crossing the wall boundaries, we place an infinite smooth wall at $z = -1.12\sigma_{LJ}$ and $z = d_g + 1.12\sigma_{LJ}$. Here infinite smooth wall is a particle-less wall that exerts a repulsive force on the monomer beads enforcing them to always remain between $z = 0$ (bottom grafting surface) and $z = d_g$ (top grafting surface); hence the infinite smooth wall has been placed below the bottom grafting surface (i.e., at $z = -1.12\sigma_{LJ}$) and above the top grafting surface (i.e., at $z = d_g + 1.12\sigma_{LJ}$). The parameters for the interactions are same as our previous work [61]. The polymers are simulated in an implicit solvent (i.e., the case where the solvent molecules are not modeled explicitly, or in other words, the interactions between the solvent molecules and polymer chains are not explicitly accounted for); however, as in our system the polymer brushes are grafted with a large grafting density, we anticipate that our simulation results would be similar to that with an explicit solvent [34] (i.e., the case where the interactions between the solvent molecules and the polymer chains are explicitly accounted for).

Simulations are carried out in the presence of the periodic boundary conditions employed in x, y directions as well as in the presence of an *NVT* ensemble. The temperature was set to $T = 1.2$ (dimensionless temperature), and isothermal conditions were maintained during the simulation using a dissipative particle dynamics (DPD) thermostat. The DPD thermostat adds a dissipative force and a random force to each particle. These forces are described in Ref. [34]. We choose a friction coefficient of $5{\tau_{LJ}}^{-1}$, and the cutoff is set to $2.24\sigma_{LJ}$. The DPD thermostat cannot efficiently maintain the isothermal condition in good-solvent conditions [67]; in order to improve the performance of the DPD thermostat, we set the cutoff of the DPD thermostat to twice the cutoff of the LJ interaction. This strategy has been suggested and implemented previously by Pastorino and Müller [68].

In our simulations, initially the two opposing plates are placed far apart so that the polymer chains grafted on these opposing plates cannot interact with each other. This configuration is equilibrated for 1.2×10^7 time steps with a time step size of $0.006\tau_{LJ}$. The polymer-brush-grafted top plate was then moved closer to the bottom plate to a distance that ensures a plate separation of d_g. Under this situation the polymer brushes from the opposing plates interacted with each other. This configuration was equilibrated for 3×10^6 time steps with a time step size of $0.006\tau_{LJ}$. To simulate the condition of the externally imposed shear, we move the beads grafted to the top plate by a constant velocity of $+v_x$, and the beads grafted to the bottom plate move with a constant velocity of $-v_x$ (therefore the shear rate is $\dot{\gamma} = 2v_x/d_g$). Under these conditions, the system is equilibrated for 10^7 time steps with a time step of $0.005\tau_{LJ}$. After this equilibration, the system is simulated for an additional 2×10^7 time steps, and data were collected for every 5000 time steps.

The shear stress f_s is calculated as $f_s = - < P_{xz} >$, where $< P_{xz} >$ is the off-diagonal component of the virial pressure tensor calculated directly by LAMMPS [69]. The viscosity η is calculated as $\eta = f_s/\dot{\gamma}$. Figures 2 and 3 show the variation of

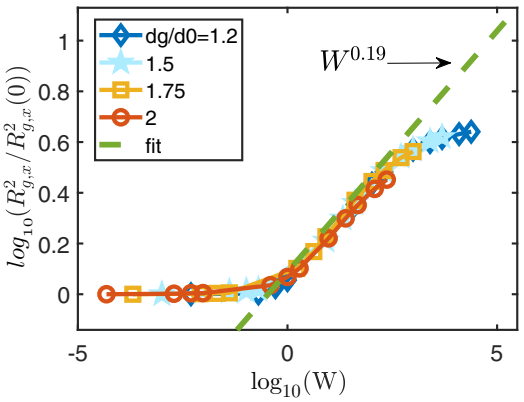

FIG. 2. MD simulation results for the variation of the ratio $R_g^2(W \gg 1)/R_0^2 = R_g^2(W \gg 1)/R_g(W \ll 1)$ (denoting the square of the shear-induced extension of the chain in the direction of the applied shear in dimensionless form) with W (Weissenberg number). The results are provided for different values of d_g/d_0 ratio (see the legend), where d_g is the gap between the two opposing plates (where the polymers are grafted) and d_0 is the unperturbed brush height. MD simulation results are shown for $1 < d_g/d_0 < 2$ signifying a weakly interpenetrating regime. From the MD simulation results, we get $R_g^2(W \gg 1)/R_g(W \ll 1) \sim W^{0.19\pm0.01}$ (i.e., including the error). In addition to the MD simulation results, we plot a line denoting $W^{0.19}$ variation.

the extension and the viscosity as function of the Weissenberg number (W). While discussing Fig. 2, we provide a detailed methodology of how we obtain the W from the shear rate $\dot{\gamma}$.

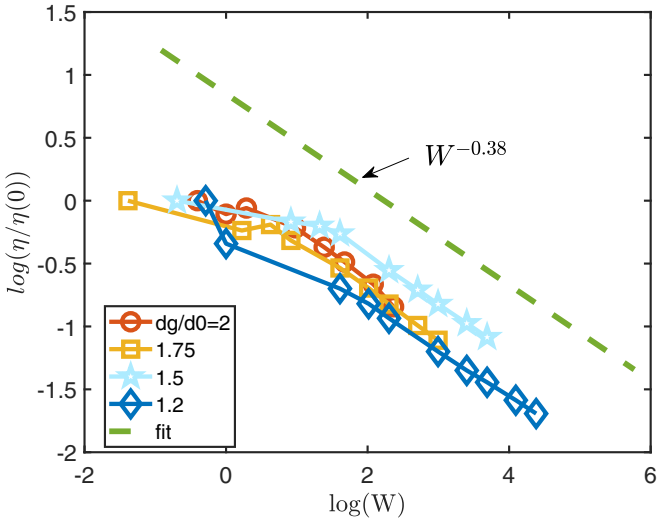

FIG. 3. MD simulation results for the variation of the ratio η/η_0 (i.e., the shear viscosity ratio) with W (Weissenberg number). The results are provided for different values of d_g/d_0 ratio (see the legend), where d_g is the gap between the two opposing plates (where the polymers are grafted) and d_0 is the unperturbed brush height. MD simulation results are shown for $1 < d_g/d_0 < 2$ signifying a weakly interpenetrating regime. From the MD simulation results, we get $\eta/\eta_0 \sim W^{-0.38\pm0.01}$ (i.e., including the error). In addition to the MD simulation results, we plot a line denoting $W^{-0.38}$ variation.

Similarly while discussing Fig. 3, we discuss the manner in which we obtain $\eta(W = 0)$.

III. MOLECULAR DYNAMICS SIMULATIONS: RESULTS

In this section, we present the results from our MD simulations for the weakly interpenetrating polymer BBLs in the presence of the applied shear ensured by subjecting the grafting surfaces (on which polymer brushes are grafted) to lateral steady-state motion.

Figure 1 provides the MD simulation snapshots for the weakly interpenetrated polymer BBLs in presence and in the absence of the shear force. We use the OVITO software package [70] to render the snapshots. We clearly witness that the presence of the shear deforms the brushes.

The response to the shear is quantified in terms of the extension R_g and the change in the viscosity η. Here R_g is same as $R_{g,x}$ i.e., the chain extension in the direction of the shear (i.e., in the x direction). Henceforth, R_g will be used to denote $R_{g,x}$. Figure 2 provides the log-log variation of the ratio of the square of the extension $R_g^2/R_0^2 = R_g^2(W \gg 1)/R_g^2(W \ll 1)$ with W. We witness $R_g^2 \sim W^{0.19}$. This suggests a significant lowering of the extension in the shear-thinning (or high W) regime in comparison to the case of the highly compressed brushes (where $R_g^2 \sim W^{0.53}$). Later during the derivation of the scaling theories, we would discuss that such a reduction in the extension for the weakly interpenetrated brushes can be attributed to the fact that the overall brush extension is dictated by the contribution of both the noninterpenetrated and the interpenetrated segments. In this context, it is useful to discuss the procedure by which we obtain W from an applied shear rate $\dot{\gamma}$. W and $\dot{\gamma}$ are related as $W = \dot{\gamma}/\dot{\gamma}^*$, where $\dot{\gamma}^* = 1/\tau$ and τ is the polymer relaxation time. Since the bilayer has a broad spectrum of the relaxation time [34], it is not easy to identify the appropriate τ that would provide us W from $\dot{\gamma}$. For this purpose, we follow the same procedure as elucidated by Galuschko *et al.* [34]. We first plot the MD results for the variation of $R_g^2/R_0^2 = R_g^2(\dot{\gamma})/R_g^2(\dot{\gamma} = 0)$ with $\dot{\gamma}$ and then shift the data such that a master curve results where there is a perfect data collapse (see Fig. 2). From this master curve, we can identify $W = 1$ as that value below which the there is no chain deformation [i.e., $R_g(\dot{\gamma}) = R_g(\dot{\gamma} = 0)$].

Figure 3 provides the log-log variation of the viscosity ratio $\eta/\eta_0 = \eta(W \gg 1)/\eta(W = 1)$ as a function of W. Here η_0 refers to the zero shear viscosity. We witness $\eta \sim W^{-0.38}$, i.e., the dependence on shear is slightly weaker as compared to that for the highly compressed regime (where $\eta \sim W^{-0.43}$). Such a behavior reflects a relatively weaker lubrication (or equivalently, a weaker lowering of the viscosity) at a high shear rate in comparison to the case of the highly compressed brushes. It is worthwhile to discuss here our strategy to obtain $\eta(W = 1)$. We first wanted to obtain $\eta(W = 0)$ and not $\eta(W = 1)$. The exact value of $\eta(W = 0)$ obtained from the MD data suffers from strong fluctuations. Therefore, following Refs. [34,35], we assume the value of $\eta(W = 0)$ to be approximately equal to $\eta(W = 1)$. Of course it should be noted here that the exact value of $\eta(W = 0)$ will not affect the scaling variation of $\eta(W)$ with W; it will simply shift the data along the y axis without changing the slope.

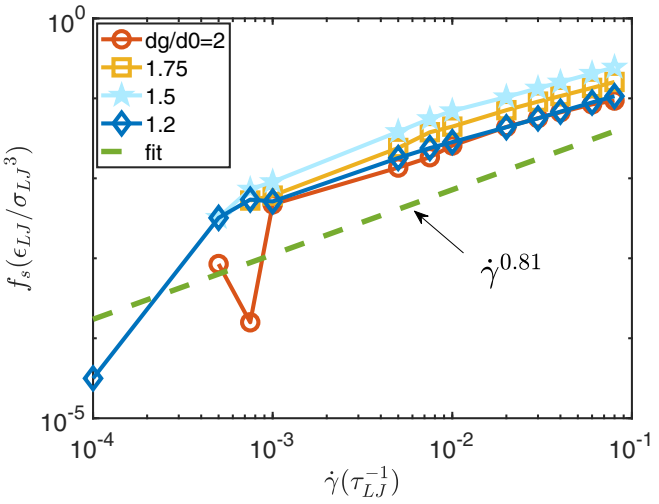

FIG. 4. MD simulation results for the $f_s - vs - \dot{\gamma}$ variation, where f_s is the shear stress (in units of $\epsilon_{LJ}/\sigma_{LJ}^3$) and $\dot{\gamma}$ is the shear rate (in units of τ_{LJ}^{-1}). The results are provided for different values of d_g/d_0 ratio (see the legend), where d_g is the gap between the two opposing plates (where the polymers are grafted) and d_0 is the unperturbed brush height. MD simulation results are shown for $1 < d_g/d_0 < 2$ signifying a weakly interpenetrating regime. From the MD simulation results, we get $f_s \sim \dot{\gamma}^{0.81\pm0.015}$ (i.e., including the error). In addition to the MD simulation results, we plot a line denoting $\dot{\gamma}^{0.81}$ variation.

Finally in Fig. 4 we show the variation of the shear stress (f_s) with the shear rate $\dot{\gamma}$, elucidating $f_s \sim \dot{\gamma}^{0.81}$. This scaling behavior persists over a wide range of shear rates, and Fig. 4 therefore confirms that even for $\dot{\gamma}$, the shear stress does not vary linearly with $\dot{\gamma}$. The scaling calculations provided below will utilize this highly nonintuitive situation where $f_s \sim \dot{\gamma}^{0.81}$.

IV. SCALING THEORIES

A. Previously obtained scaling expressions for weakly interpenetrated polymer BBLs

We first reexpress certain scaling behavior witnessed for weakly interpenetrated polymer brush bilayers. Most of the expressions provided in this subsection have already been derived in our previous paper [61], but we repeat them here for the sake of completeness.

As we are studying a weakly interpenetrated polymer BBL, a part of the polymer molecule is in the interpenetrated domain while the other part is outside the interpenetrated domain. The part that is in the interpenetrated domain can be considered to be described as blob-encased segments [61,62]. Following Kreer and Balko [42], we can express the interaction energy per unit area for the interpenetrated semidilute polymer BBLs as

$$A \sim n_i k_B T, \tag{1}$$

where $k_B T$ is the thermal energy and n_i is the number density of blobs (having the units of $1/m^2$) within the interpenetration (IP) zone expressed as

$$n_i = c_\delta \delta / g_c. \tag{2}$$

Here δ is the IP length, c_δ is the monomer concentration in the IP zone, and g_c is the number of monomers present in each blob. Considering N_1 number of monomers are outside the IP zone and $N - N_1$ monomers are inside the IP zone, we can express [61]

$$c_\delta \sim \frac{(N - N_1)\sigma_g}{\delta} \sim \frac{N(2-x)\sigma_g}{\delta}, \tag{3}$$

$$g_c \sim \left(\frac{\xi_c}{a}\right)^{1/\nu}, \tag{4}$$

$$\xi_c \sim a(c_\delta a^3)^{\nu/(1-3\nu)}, \tag{5}$$

where a is the Kuhn length (a polymer molecule can be assumed to be made of several freely jointed segments, which are known as the Kuhn segments, and the length of each segment is the Kuhn length), σ_g is the grafting density, $x = 1 + N_1/N$, g_c is the number of monomers in each blob, ξ_c is the blob radius, and ν is the Flory exponent (this exponent expresses the radius of gyration of a coiled polymer chain as a function of the number of monomers and the solvent quality). Of course, following our previous paper [61] we get a new scaling expression for the IP length δ for the weakly interpenetrated semidilute polymer BBLs as

$$\delta \sim a[N^{1-\nu}(2-x)^{2\nu}(a^2\sigma_g)^{(7-15\nu)/3}]^{1/(5\nu-1)}. \tag{6}$$

We arrive at Eq. (6) This expression for δ is distinctly different from that of the strongly compressed regime [21].

Using Eqs. (3) and (6) in Eq. (5), we can eventually write

$$\xi_c \sim a N^{\frac{2\nu}{1-5\nu}}(2-x)^{\frac{\nu}{1-5\nu}}(\sigma_g a^2)^{\frac{10\nu}{3(1-5\nu)}}. \tag{7}$$

Furthermore, using Eqs.(3), (4), (6), and (7) in Eq. (2), we can write

$$n_i \sim a^{-2} N^{\frac{1+5\nu}{5\nu-1}}(2-x)^{\frac{5\nu}{5\nu-1}}(\sigma_g a^2)^{\frac{7+15\nu}{3(5\nu-1)}}. \tag{8}$$

Consequently, we may express the per unit area interaction energy as

$$A \sim k_B T a^{-2} N^{\frac{1+5\nu}{5\nu-1}}(2-x)^{\frac{5\nu}{5\nu-1}}(\sigma_g a^2)^{\frac{7+15\nu}{3(5\nu-1)}}, \tag{9}$$

which in turn helps to express the per unit area compressive force f_c as

$$f_c \sim -\frac{\partial A}{\partial d_g} = -\frac{\partial A}{\partial x}\frac{dx}{d(d_g)}$$
$$\sim \frac{k_B T}{d_0} a^{-2} N^{\frac{1+5\nu}{5\nu-1}}(2-x)^{\frac{1}{5\nu-1}}(\sigma_g a^2)^{\frac{7+15\nu}{3(5\nu-1)}}. \tag{10}$$

B. Relaxation time

The relaxation time of the polymer brush can be expressed as [considering $\tau_{\text{melt,highly compressed}} = \Gamma a^2 N^2/(k_B T)$ [21] and replacing a by ξ_c, N by $(N - N_1)/g_c$ and Γ (friction constant of a blob) by $\eta_s \xi_c$ (η_s is the solvent viscosity)]

$$\tau \sim \frac{\eta_s \xi_c^3}{k_B T}\left(\frac{N - N_1}{g_c}\right)^2. \tag{11}$$

Using Eq. (4) to replace g_c and Eq. (7) to replace ξ_c, we can obtain

$$\tau \sim \frac{\eta_s a^3}{k_B T} N^{\frac{4\nu+2}{5\nu-1}}(2-x)^{\frac{7\nu}{5\nu-1}}(\sigma_g a^2)^{\frac{10(3\nu-2)}{3(1-5\nu)}}. \tag{12}$$

C. Scaling of η/η_0

As established by our MD studies (Fig. 4), we can consider that the shear stress f_s does not vary linearly with the shear rate $\dot{\gamma}$ even for weak values of $\dot{\gamma}$. Rather $f_s \sim \dot{\gamma}^b$, where $b = 0.81$ (Fig. 4). Consequently,

$$f_s \sim n_i \xi_c \eta_s (\dot{\gamma} d_g)^b \sim \frac{\eta_s \dot{\gamma}^b d_g^b}{a} N^{\frac{1+3\nu}{5\nu-1}} (2-x)^{\frac{4\nu}{5\nu-1}} (\sigma_g a^2)^{\frac{7+5\nu}{3(5\nu-1)}}. \quad (13)$$

For critical shear stress (i.e., the shear stress corresponding to the critical shear rate, or the shear rate for which $W = 1$), $f_s(W = 1)$, we can replace $\dot{\gamma}$ by $1/\tau$ [where Eq. (12) provides τ] yielding

$$f_s(W=1) \sim \frac{\eta_s \tau^{-b} d_g^b}{a} N^{\frac{1+3\nu}{5\nu-1}} (2-x)^{\frac{4\nu}{5\nu-1}} (\sigma_g a^2)^{\frac{7+5\nu}{3(5\nu-1)}} \sim \eta_s^{1-b} a^{-1-3b} d_g^b (k_B T)^b N^{\frac{1+3\nu-(4\nu+2)b}{5\nu-1}} (2-x)^{\frac{4\nu-7\nu b}{5\nu-1}} \times (\sigma_g a^2)^{\frac{7+5\nu-10b(3\nu-2)}{3(5\nu-1)}}. \quad (14)$$

On the other hand, for large shear rate, we can write

$$f_s(W \gg 1) \sim N(2-x)^\beta, \quad (15)$$

which suggests that the interpenetrated segments of polymer molecule also attain a brushlike configuration. Note that here we have $f_s(W \gg 1) \sim N(2-x)^\beta$ and not $f_s(W \gg 1) \sim N$ (which occurs for fully interpenetrated brushes; see Kreer [21]) since here the shear stress is witnessed only in the interpenetrated regime. The exponent β accounts for the possible decrease in the IP due to shear.

Of course, following Kreer [21] we can write

$$f_s(W \gg 1) = f_s(W=1) W^k, \quad (16)$$

where using Eq. (12), we can write

$$W^k \sim (\dot{\gamma}\tau)^k \sim \frac{\eta_s^k a^{3k}}{(k_B T)^k} N^{\frac{k(4\nu+2)}{5\nu-1}} (2-x)^{\frac{7\nu k}{5\nu-1}} (\sigma_g a^2)^{\frac{10k(3\nu-2)}{3(1-5\nu)}}. \quad (17)$$

Using Eqs. (14), (15), and (17) in Eq. (16) and balancing the exponents of N and $2-x$, we can finally write

$$k - b = \frac{\nu - 1}{2\nu + 1}, \quad \text{(Balancing the exponent of } N\text{)} \quad (18)$$

$$\beta = \frac{7\nu(k-b) + 4\nu}{5\nu - 1}. \quad \text{[Balancing the exponent of } (2-x)\text{]} \quad (19)$$

From Eq. (18) we obtain (using $\nu \approx 0.588$ and $b = 0.81$; see Fig. 4)

$$k = 0.62 \quad (20)$$

On the other hand, from Eq. (19), we can write

$$\beta = 0.81, \quad (21)$$

which confirms the lowering of the IP. Following Spirin *et al.* [35] and using Eq. (20), we can finally write

$$\frac{\eta}{\eta_0} \sim \frac{1}{W} \frac{f_s(W \gg 1)}{f_s(W=1)} \sim W^{k-1} \sim W^{-0.38}; \quad (22)$$

i.e., we get a perfect match with the MD results.

D. Scaling of $R^2(W \gg 1)/R_0^2$

We now consider the scaling of $R^2(W \gg 1)/R_0^2$ [here $R(W \gg 1)$ represents the stretching in the direction of the shear]. We can express R_0 as the sum of the interpenetrated and noninterpenetrated (which forms a brush) segments yielding

$$R_0 = R(W \ll 1) \sim \Xi_1 a N^\nu (2-x)^\nu + \Xi_2 b N. \quad (23)$$

Variation of Ξ_1 and Ξ_2 dictates the extent of IP: no IP would imply $\Xi_1 = 0$ and $\Xi_2 = 1$, whereas maximum penetration would imply $\Xi_2 = 0$ and $\Xi_1 = 1$ and $x = 0$.

Second, we can write

$$R(W \gg 1) \sim N, \quad (24)$$

implying that the interpenetrated part also forms a brushlike configuration. Of course, here too we use the relationship presented by Kreer [21],

$$R(W \gg 1) \sim R(W \ll 1) W^\alpha, \quad (25)$$

where using Eq. (12), we can write

$$W^\alpha \sim (\dot{\gamma}\tau)^\alpha \sim \frac{\eta_s^\alpha a^{3\alpha}}{(k_B T)^\alpha} N^{\frac{\alpha(4\nu+2)}{5\nu-1}} (2-x)^{\frac{7\nu\alpha}{5\nu-1}} (\sigma_g a^2)^{\frac{10\alpha(3\nu-2)}{3(1-5\nu)}}. \quad (26)$$

Therefore, using Eqs. (23), (24), and (26) in Eq. (25), we can write by balancing the powers of N and considering $\nu \approx 0.588$

$$(\alpha)_{\Xi_2=0} = \frac{(1-\nu)(5\nu-1)}{4\nu+2} \approx 0.18 \ \text{(full IP)}, \quad (\alpha)_{\Xi_1=0} = 0 \ \text{(no IP)}. \quad (27)$$

We can therefore consider an average α in the weakly interpenetrated domain as

$$\alpha \approx \frac{(\alpha)_{\Xi_2=0} + (\alpha)_{\Xi_1=0}}{2} \approx 0.09. \quad (28)$$

Therefore, following Spirin *et al.* [35] and Kreer [21] and Eq. (28) we can write

$$\frac{R^2(W \gg 1)}{R_0^2} \sim \frac{R^2(W \gg 1)}{R^2(W \ll 1)} \sim W^{2\alpha} \sim W^{0.18}; \quad (29)$$

i.e., here too we get a wonderful match with the MD simulation results.

V. CONCLUSIONS

In this paper, we study the shearing of weakly interpenetrated polymer brushes and identify scaling regimes that are significantly deviated from the well-studied case of highly compressed polymer brushes. Our findings point to a weakened lubricity effect and a significantly reduced stretching behaviors compared to that witnessed in the highly compressed regimes. We explain these findings through a detailed scaling theory that matches nicely with the MD predictions. In fact, a key component of this scaling theory, motivated by the MD predictions, is a consideration that even at weak W, the shear stress varies nonlinearly with the shear rate. The scaling calculations also assume that the overall stretching is dictated by the behavior of

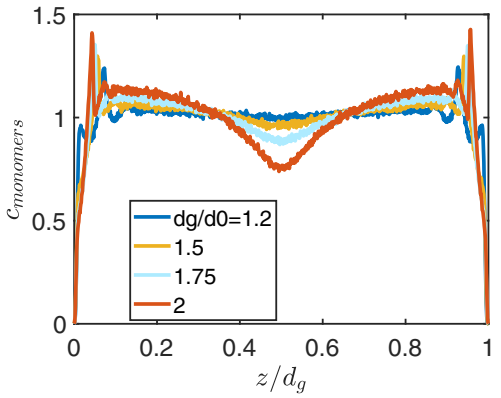

FIG. 5. Variation in the monomer density profile across the channel for different values of d_g/d_0 (shown in the legend).

both the interpenetrated and the noninterpenetrated segments of the polymer brush. Overall this study sheds light on the lubricity and shearing action of the polymer BBLs in a domain that has remained hitherto unexplored.

As has been already discussed above, our scaling theory is based on the condition (motivated by the findings of the MD simulations that) shear stress $f_s \sim \dot{\gamma}^{0.81}$. This is very counterintuitive since we work with a small shear rate and at such conditions one would expect that f_s should vary linearly with $\dot{\gamma}$. Possibly, such a nonlinear variation (quantified by this exponent 0.81) arises due to the fact that at the small shear rates that we are applying it becomes difficult to equilibrate a sheared system. Another issue with our derivation is that we assume that the segment of the polymer brush that is in the interpenetrated regime is encased in blobs of uniform size (characterizing a uniform monomer density in the interpenetrated regime). Such a situation is not strictly correct especially for large (close to 2) values of d_g/d_0 (i.e., where the degree of IP decreases), as is evident from Fig. 5. Due to these above two reasons, there can be a possibility that this wonderful match between the scaling approach and the MD data is coincidental.

Finally, we would like to point out that no experiments have conducted the shear experiments for such a weakly interpenetrated polymer brush bilayer system. However, experiments based on surface forces apparatus (SFA) have carried out shear force measurements between the polystyrene chains grafted to opposing surfaces for larger degrees of IP [55]. Similarly, SFA-based experiments have quantified compressive forces for both large and weak IP [31]. Approaches highlighted in these two studies can be easily coupled to carry out the SFA-based experiments to pinpoint the shear stress, chain extension, and shear viscosity in weakly interpenetrated polymer brush bilayer system.

ACKNOWLEDGMENTS

The authors would like to acknowledge NHLBI/NIH-UMD graduate partnership program for partially supporting P.D. The authors would also like to acknowledge the High Performance Computing Facilities (Deepthought 2) at the University of Maryland. Finally, the authors would like to acknowledge Shayandev Sinha for useful discussions.

APPENDIX: VARIATION OF THE MONOMER DENSITY PROFILE

Figure 5 shows the variation of the monomer density profile in absence of the shear. As the degree of IP decreases, i.e., d_g/d_0 increases and approaches 2, we find that the monomer density in the channel center decreases, establishing the nonuniformity in the monomer concentration (or the nonuniformity in the size of the hypothetical blobs used to describe the IP zone).

[1] S. Alexander, J. Phys. **38**, 977 (1977).
[2] P. G. de Gennes, J. Phys. (Paris) **37**, 1445 (1976).
[3] P.-G. de Gennes, Macromolecules **13**, 1069 (1980).
[4] R. R. Netz and D. Andelman, Phys. Rep. **380**, 1 (2003).
[5] S. Das, M. Banik, G. Chen, S. Sinha, and R. Mukherjee, Soft Matt. **11**, 8550 (2015).
[6] S. T. Milner, Science **251**, 905 (1991).
[7] K. Knop, R. Hoogenboom, D. Fischer, and U. S. Schubert, Angew. Chem. Intl. Ed. **49**, 6288 (2010).
[8] J. S. Suk, Q. Xu, N. Kim, J. Hanes, and L. M. Ensign, Adv. Drug Deliv. Rev. **99**, 28 (2016).
[9] H. Shamsi Jazeyi, C. A. Miller, M. S. Wong, J. M. Tour, and R. Verduzco, J. Appl. Polym. Sci. **131**, 40576 (2014).
[10] J. O. Zoppe, R. A. Venditti, and O. J. Rojas, J. Colloid Interf. Sci. **369**, 202 (2012).
[11] C. Jiang, Y. Zhang, Q. Wang, and T. Wang, J. Appl. Polym. Sci. **129**, 2959 (2013).
[12] H. Suzuki, M. Murou, H. Kitano, K. Ohno, and Y. Saruwatari, Colloid. Surf. B **84**, 111 (2011).
[13] G. W. de Groot, M. G. Santonicola, K. Sugihara, T. Zambelli, E. Reimhult, J. Vrös, and G. J. Vancso, ACS Appl. Mater. Interf. **5**, 1400 (2013).
[14] B. Yameen, M. Ali, R. Neumann, W. Ensinger, W. Knoll, and O. Azzaroni, J. Am. Chem. Soc. **131**, 2070 (2009).
[15] M. Ali, B. Yameen, R. Neumann, W. Ensinger, W. Knoll, and O. Azzaroni, J. Am. Chem. Soc. **130**, 16351 (2008).
[16] M. Ali, B. Schiedt, R. Neumann, and W. Ensinger, Macromol. Biosci. **10**, 28 (2010).
[17] S. Umehara, M. Karhanek, R. W. Davis, and N. Pourmand, Proc. Natl. Acad. Sci. USA **106**, 4611 (2009).
[18] M. Ali, B. Yameen, J. Cervera, P. Ramirez, R. Neumann, W. Ensinger, W. Knoll, and O. Azzaroni, J. Am. Chem. Soc. **132**, 8338 (2010).
[19] B. Vilozny, A. L. Wollenberg, P. Actis, D. Hwang, B. Singaram, and N. Pourmand, Nanoscale **5**, 9214 (2013).
[20] M. Ali, P. Ramirez, S. Mafe, R. Neumann, and W. Ensinger, ACS Nano **3**, 603 (2009).
[21] T. Kreer, Soft Matt. **12**, 3479 (2016).
[22] J. Klein, D. Perahia, and S. Warburg, Nature (London) **352**, 143 (1991).
[23] H. J. Taunton, C. Toprakcioglu, L. J. Fetters, and J. Klein, Nature (London) **332**, 712 (1988).
[24] J. Klein, Colloids Surf. A **86**, 63 (1994).

[25] R. Tadmor, J. Janik, J. Klein, and L. J. Fetters, Phys. Rev. Lett. **91**, 115503 (2003).
[26] S. de Beer, G. D. Kenmoé, and M. H. Müser, Friction **3**, 148 (2015).
[27] S. de Beer and M. H. Müser, Macromolecules **47**, 7666 (2014).
[28] S. de Beer, E. Kutnyanszky, P. M. Schön, G. J. Vancso, and M. H. Müser, Nat. Commun. **5**, 3781 (2014).
[29] J.-M. Y. Carrillo, D. Russano, and A. V. Dobrynin, Langmuir **27**, 14599 (2011).
[30] J.-M. Y. Carrillo, W. M. Brown, and A. V. Dobrynin, Macromolecules **45**, 8880 (2012).
[31] S. M. Balko, T. Kreer, P. J. Costanzo, T. E. Patten, A. Johner, T. L. Kuhl, and C. M. Marques, PLoS ONE **8**, e58392 (2009).
[32] J. Klein, Science **323**, 47 (2009).
[33] T. Moro, Y. Takatori, K. Ishihara, T. Konno, Y. Takigawa, T. Matsush, U. Chung, K. Nakamura, and H. Kawaguchi, Nat. Mater. **3**, 829 (2004).
[34] A. Galuschko, L. Spirin, T. Kreer, A. Johner, C. Pastorino, J. P. Wittmer, and J. Baschnagel, Langmuir **26**, 6418 (2010).
[35] L. Spirin, A. Galuschko, T. Kreer, A. Johner, J. Baschnagel, and K. Binder, Eur. Phys. J. E **33**, 307 (2010).
[36] T. Kreer, M. H. Müser, K. Binder, and J. Klein, Langmuir **17**, 7804 (2001).
[37] G. S. Grest, Adv. Polym. Sci. **138**, 149 (1999).
[38] M. Murat and G. S. Grest, Phys. Rev. Lett. **63**, 1074 (1989).
[39] T. Kreer, K. Binder, and M. H. Müser, Langmuir **19**, 7551 (2003).
[40] L. Chen, H. Merlitz, S.-Z. He, C.-X. Wu, and J.-U. Sommer, Macromolecules **44**, 3109 (2011).
[41] L. Spirin, A. Galuschko, and T. Kreer, Macromolecules **44**, 9399 (2011).
[42] T. Kreer and S. M. Balko, ACS Macro Lett. **2**, 944 (2013).
[43] V. M. Amoskov, T. M. Birshtein, and V. A. Pryamitsyn, Macromolecules **31**, 3720 (1998).
[44] A. Chakrabarti, P. Nelson, and R. Toral, J. Chem. Phys. **100**, 748 (1994).
[45] A. Wynveen and C. N. Likos, Phys. Rev. E **80**, 010801(R) (2009).
[46] T. A. Witten, L. Leibler, and P. A. Pincus, Macromolecules **23**, 824 (1990).
[47] H. Ohshima, Adv. Colloid Interf. Sci. **226**, 2 (2015)
[48] H. Ohshima, Colloid Polym. Sci. **292**, 431 (2014).
[49] G. S. Grest, Phys. Rev. Lett. **76**, 4979 (1996).
[50] I. G. Elliott, T. L. Kuhl, and R. Faller, J. Phys. Chem. B **117**, 4134 (2013).
[51] M. K. Singh, P. Ilg, R. M. Espinosa-Marzal, M. Kröger, and N. D. Spencer, Langmuir **31**, 4798 (2015).
[52] D. Russano, J-M. Y. Carrillo, and A. V. Dobrynin, Langmuir **27**, 11044 (2011).
[53] A. G. Goicochea, E. Mayoral, J. Klapp, and C. Pastorino, Soft Matter **10**, 166 (2014).
[54] A. Erbas and J. Paturej, Soft Matter **11**, 3139 (2015).
[55] P. A. Schorr, T. C. B. Kwan, S. M. Kilbey II, E. S. G. Shaqfey, and M. Tirrell, Macromolecules **36**, 389 (2003).
[56] E. Eiser and J. Klein, Macromolecules **40**, 8455 (2007).
[57] L. Tsarkova, X. Zhang, N. Hadjichristidis, and J. Klein, Macromolecules **40**, 2539 (2007).
[58] O. Tairy, N. Kampf, M. J. Driver, S. P. Armes, and J. Klein, Macromolecules **48**, 140 (2015).
[59] R. Krishnamoorti and E. P. Giannelis, Langmuir **17**, 1448 (2001).
[60] C. M. Wijmans and B. Smit, Macromolecules **35**, 7138 (2002).
[61] P. R. Desai, S. Sinha, and S. Das, Soft Matt. **13**, 4159 (2017).
[62] P. R. Desai, S. Sinha, and S. Das, Phys. Rev. E **97**, 032503 (2018).
[63] S. Plimpton, J. Comput. Phys. **117**, 1 (1995).
[64] G. S. Grest and K. Kremer, Phys. Rev. A **33**, 3628(R) (1986).
[65] K. Kremer and G. S. Grest, J. Chem. Phys. **92**, 5057 (1990).
[66] R. Everaers, S. K. Sukumaran, G. S. Grest, C. Svaneborg, A. Sivasubramanian, and K. Kremer, Science **303**, 823 (2004).
[67] C. Pastorino, T. Kreer, M. Müller, and K. Binder, Phys. Rev. E **76**, 026706 (2007).
[68] C. Pastorino and M. Müller, J. Chem. Phys. **140**, 014901 (2014).
[69] A. P. Thompson, S. J. Plimpton, and W. Mattson, J. Chem. Phys. **131**, 154107 (2009).
[70] A. Stukowski, Modelling Simul. Mater. Sci. Eng. **18**, 085001 (2010).